ACCELERATED FATIGUE CRACK GROWTH BEHAVIOR OF PWA 1480 SINGLE CRYSTAL ALLOY AND ITS DEPENDENCE ON THE DEFORMATION MODE

Jack Telesman and Louis J. Ghosn*

NASA Lewis Research Center
Cleveland Ohio, USA 44135

Abstract

An investigation of the fatigue crack growth (FCG) behavior of PWA 1480 single crystal nickel base superalloy was conducted. Typical Paris region behavior was observed above a ΔK of 8 MPa$\sqrt{m}$. However, below that stress intensity range, the alloy exhibited highly unusual behavior. This behavior consisted of a region where the crack growth rate became essentially independent of the applied stress intensity. The transition in the FCG behavior was related to a change in the observed crack growth mechanisms. In the Paris region, fatigue failure occurred along {111} facets, however at the lower stress intensities, (001) fatigue failure was observed. A mechanism was proposed, based on barriers to dislocation motion, to explain the changes in the observed FCG behavior. The FCG data were also evaluated in terms of a recently proposed stress intensity parameter, K_{rss}. This parameter, based on the resolved shear stresses on the slip planes, quantified the crack driving force as well as the mode I ΔK, and at the same time was also able to predict the microscopic crack path under different stress states.

Introduction

The relatively recent advent of the directionally solidified and single crystal nickel based superalloys for aerospace applications has focused attention on the ability to understand and predict the fatigue behavior of these alloys. In particular, with the recent emphasis on damage tolerant design for turbine engine components, the understanding and modeling of fatigue crack growth (FCG) behavior has become increasingly important.

Stress intensity range (ΔK) has been used for the past 25 years as the correlating parameter for fatigue crack growth. It has shown to be a good empirical parameter for correlating the FCG data of polycrystalline materials. While this crack driving force parameter is well suited for polycrystalline alloys, it may not be the best parameter to use for very large grain or single crystal alloy FCG data correlation. Studies in the recent years have shown that short cracks exhibit lower threshold stress intensities and accelerated FCG rates in comparison to long cracks when compared at similar values of ΔK (1-5). The short crack behavior is usually limited to a situation where the crack size is of the same order of magnitude or smaller than the grain size (3-5). This points to the weakness of the ΔK parameter to correlate the FCG data when the grain orientation and microstructure become important factors in controlling FCG behavior.

* Resident Research Associate

Superalloys 1988
Edited by S. Reichman, D.N. Duhl,
G. Maurer, S. Antolovich and C. Lund
The Metallurgical Society, 1988

In addition to pointing out the weaknesses of the use of the ΔK parameter, the above discussion underscores the importance of microstructure and the associated deformation mechanisms in controlling FCG behavior. A single crystal alloy offers the best opportunity to study in detail the effect of microstructure and the deformation mechanisms on the FCG behavior. For a single crystal alloy, the deformation mechanisms are active on a substantially larger scale, making their observation and identification considerably easier. In addition, the grain orientation of a single crystal can be easily determined allowing for detailed calculations of the stresses on the active slip systems.

Chen and Liu (6) recently proposed a crack driving force parameter for correlating FCG data. The new parameter, also with its roots in linear elastic fracture mechanics, is based on the resolved shear stresses on the active slip plane. This parameter may be a better candidate than ΔK for the correlation of FCG data since it takes into account the deformation mechanisms and the actual crack path.

A test program was undertaken to determine the FCG behavior of a single crystal alloy in the near-threshold and intermediate ΔK region. The alloy chosen was a single crystal nickel based superalloy PWA 1480. The emphasis was placed in relating the fatigue damage mechanisms to the observed crack growth behavior. The shear stress intensity parameter proposed by Chen and Liu (6) was evaluated for correlation with the FCG data.

Experimental Procedure

Single crystal PWA 1480 slabs were obtained with the following composition in weight percent: 4.7 Al, 0.005 C, 4.8 Co, 9.4 Cr, 0.9 Si, 11 Ta, 1. Ti, 5.2 W and the balance in Ni. The slabs were solution treated for 4 hr at 1290°C, followed by the usual coating cycle diffusion treatment of 1080°C for 4 hr and aging at 870°C for 32 hr. The diffusion treatment was used to simulate the typically performed heat treatment, even though the specimens were uncoated. The alloy contained 60 to 65 vol % of the γ' phase, which has a cuboidal morphology and a cube size range between 0.4-0.6μm (7).

Five compact tension specimens were machined with the loading axis being 7° from the (001) orientation and the side faces of the specimens in the near (010) orientation as shown schematically in Fig. 1. In order to avoid crack closure effects, the testing was performed at a load ratio R (min load/max load) of 0.5. Three specimens were tested to achieve the near-threshold region by using a load shedding procedure recommended by ASTM (8). Crack length and crack closure were measured through the use of the compliance method and the crack length was also verified through occasional optical measurements. After the near threshold region was achieved, the tests were restarted using a constant load range mode, also at R=0.5, to obtain a ΔK increasing data base. This was done to assure that load shedding had no effect on FCG data. Two other specimens were tested only at a constant load range mode to achieve a FCG data base in the intermediate ΔK region. All the tests, with one exception, were conducted in laboratory environment and at room temperature. One test in the near threshold region was conducted in a nitrogen atmosphere to analyze any possible environmental effects on FCG behavior. All the testing was done at a frequency of 20 Hz. For comparison purposes, three additional tests were performed on a readily available polycrystalline nickel base superalloy. These tests were performed on specimens machined from a polycrystalline Waspaloy disk forging under test conditions identical to those of PWA 1480, with the exception that no nitrogen testing was performed.

The stress and displacement fields, along a given crack path, were determined for FCG data correlation using the two dimensional boundary integral equation (BIE) method (9). The two surfaces of the crack are modeled in separate subregions with appropriate continuity along the interface. A typical two dimensional multidomain BIE mesh for the compact tension specimen

is shown in Fig. 2. The number of elements and the rigid body constraints are also shown. Quadratic variations of the displacements and tractions are assumed. An isotropic solution is used since it has been shown by Chan and Cruse (10) that the difference between anisotropic and isotropic solutions are neglegible for the single crystal nickel based superalloy. The shear stress intensity factor parameter was determined from the stress field solution near the crack tip by the projection of the traction on a slip plane in the direction of slip, as proposed by Chen and Liu (6). This procedure is explained in more detail in a later section .

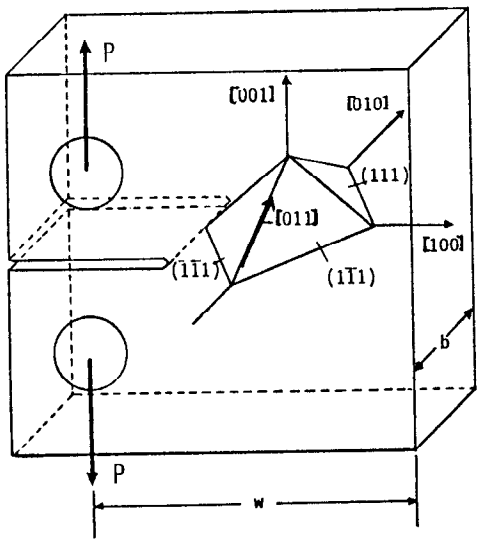

Fig. 1 Approximate orientation of {111} planes with respect to the compact tension specimens tested.

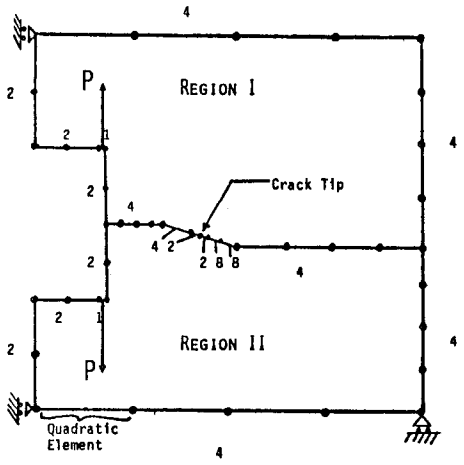

Fig. 2 Two-dimensional multidomain boundary integral mesh.

Results

Macroscopic Observations of Failed Specimens

For all the PWA 1480 specimens tested, the macroscopic failure planes were approximately 7° to the plane of the starter notch. Thus the macroscopic failure occurred on the (001) plane. Small amounts of secondary cracking were observed on the {111} type planes at higher stress intensity ranges. The Waspaloy specimens failed in the plane of the starter notch.

Fatigue Crack Growth Results

Chan and Cruse (10) have shown that the ASTM stress intensity solution for a Mode I crack is valid for single crystal compact tension specimens having an inclined crack, provided that the crack angle is less than 30° from the starter notch. The PWA 1480 specimens tested exhibited only a 7° crack angle, thus Mode I solutions were used to correlate the FCG data.

The PWA 1480 fatigue crack growth data is shown in Fig. 3. At stress intensities above a ΔK of approximately 8 MPa$\sqrt{m}$, the FCG behavior is rather normal, exhibiting typical region II (Paris region) characteristics where the crack growth rate is directly proportional to the applied ΔK, on a log-log basis. However, below that value, the observed behavior is very different in comparison to the typical long crack behavior. Below a ΔK of 8 MPa$\sqrt{m}$, the FCG rate becomes essentially independent of the applied ΔK. This region continues until a ΔK of approximately 2.5 MPa$\sqrt{m}$ is reached, after which the FCG rate again starts decreasing with decreasing ΔK. This behavior was identical under both the load shedding and constant load portions of the test, indicating that the test procedure was not a factor in causing

this behavior. Crack closure was monitored throughout the test and was shown to be below that of K_{min}, thus it also had no effect on the test results. The results of the test performed in nitrogen, shown in Fig. 4, reveal identical behavior indicating that the environment is probably not the cause of this unusual behavior.

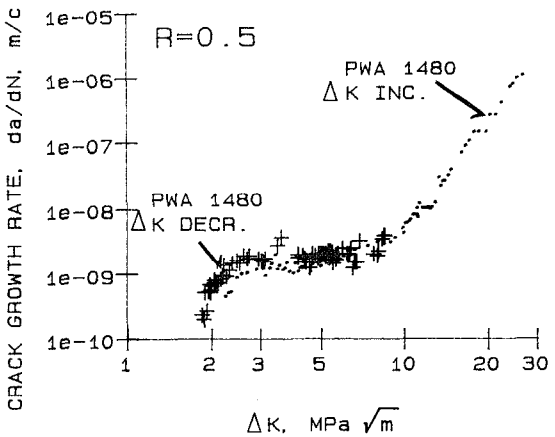

Fig. 3 Fatigue crack growth rate of PWA 1480 as a function of ΔK.

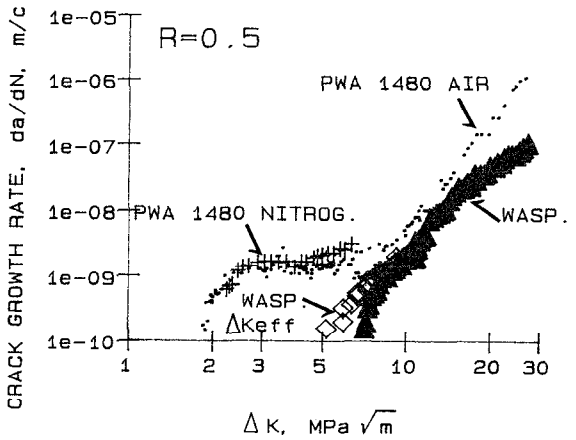

Fig. 4 Comparison of FCG rates of PWA 1480 and Waspaloy.

A comparison of the FCG behavior of PWA 1480 and Waspaloy is also shown in Fig. 4. Waspaloy FCG behavior is quite different and resembles that of typically observed long crack growth curves. For Waspaloy, in the near threshold regime, the crack closure stress intensity factor, K_{cl}, was reached at K values somewhat above the K_{min}. The data was corrected for crack closure and is also shown in Fig. 4 based on the effective ΔK, (ΔK_{eff}). The corrected data still exhibits the typically observed FCG trends.

Review of the literature failed to reveal any previous observations in a polycrystalline alloy under prevailing linear elastic conditions, which are similar to the observed PWA 1480 behavior. Nor was any near-threshold single crystal data found in the literature to which the current results could be compared.

The region of unusual FCG behavior of PWA 1480 is similar in appearance to the accelerated crack growth behavior reported for short cracks (1-5). Whether this similarity is coincidental or whether it is an indication of a single phenomenon is a topic for future studies.

Fractography of PWA Specimens

A detailed fractographic evaluation was performed on the PWA 1480 specimens to determine the microscopic deformation modes and their relationship to the observed FCG behavior.

Outside Surface Fractography: Even though on the macroscopic level the crack propagated on the (001) plane inclined 7° to the starter notch, the surface observations on the microscopic level revealed a presence of slip traces ±45° to the macroscopic crack (or 52° and -38° to the starter notch). Thus crack propagation was a result of slip on at least two different planes as shown in Fig. 5.

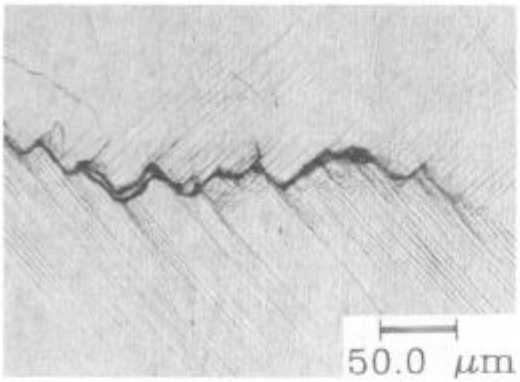

a) General behavior

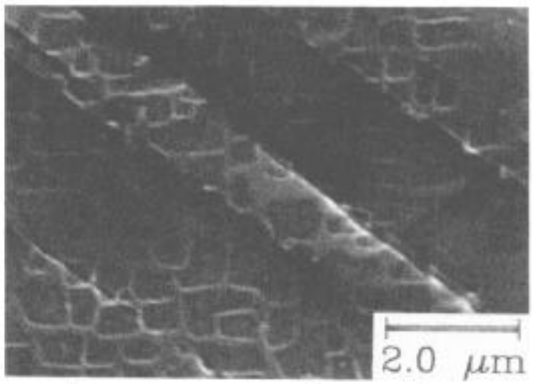

b) Slip offsets (etched)

Fig. 5 Outside surface observations of the crack growth process.

Through-Thickness Fractography: Fig. 6 reveals the progressive change in the fatigue failure mechanism as a function of the applied stress intensity in the mid-thickness of the specimens. At the lowest stress intensities (Fig. 6a), cuboidal facets of the strengthening precipitates are seen throughout the mid-thickness sections resulting in a (001) fatigue failure appearance. As the stress intensity was increased, areas containing facets on {111} planes also became apparent (Fig. 6b). With a further increase in the stress intensity, the (001) fatigue failure completely disappeared, and was replaced by the {111} fatigue failure (Fig. 6c-d). As seen in these figures, the increase in the ΔK resulted in an increase in the size of the {111} failure facets. Also, in the mid-thickness areas the failure occurred on all four {111} planes.

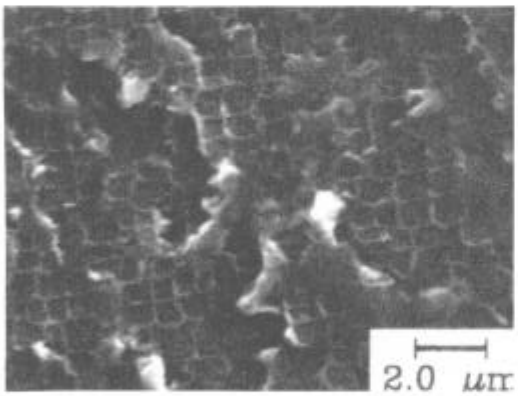

a) ΔK=2.2 MPa$\sqrt{m}$ (etched)

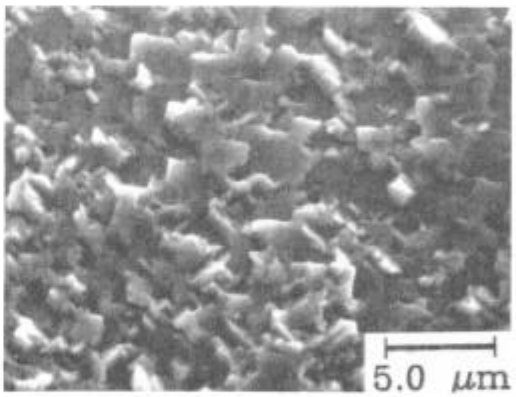

b) ΔK=8.9 MPa$\sqrt{m}$

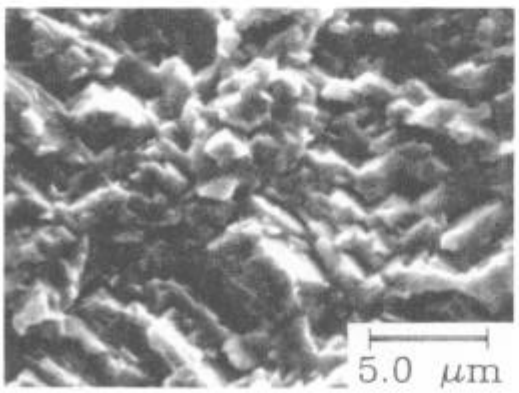

c) ΔK=18.5 MPa$\sqrt{m}$

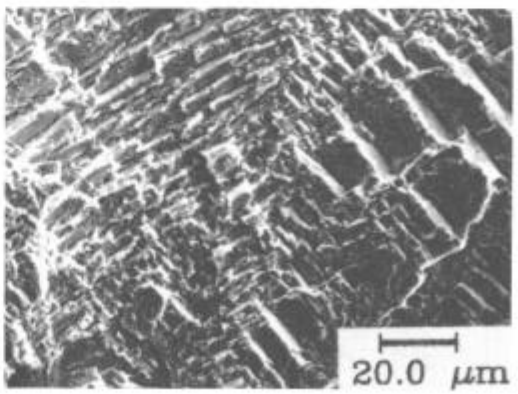

d) Final failure ΔK>40 MPa$\sqrt{m}$

Fig. 6 Mid-thickness failure appearance at various ΔK.

An interesting phenomenon was observed with regard to the (001) fatigue failure. Examination of the small ridges (or steps) on the etched failure surface, as viewed in Fig. 6a and at a higher magnification in Fig. 7, suggests that the failure was confined only to the matrix phase. The results obtained by Miner et al (11) can be used to support the above suggestion. They have shown that only octahedral {111} slip is active for a (001) oriented single crystal at room temperature. Since no {111} facets were visible on the failure surface at low ΔK, and [001] cube slip is unlikely, the only plausible mechanism which could explain the presence of (001) γ' cuboidal facets on the failure surface is the confinement of the {111} slip deformation to the matrix network. The {111} matrix slip deformation cannot be resolved without transmission electron microscopy (TEM). A hypothesis explaining why such mechanism is occurring and its influence on the FCG behavior is described later on in the paper.

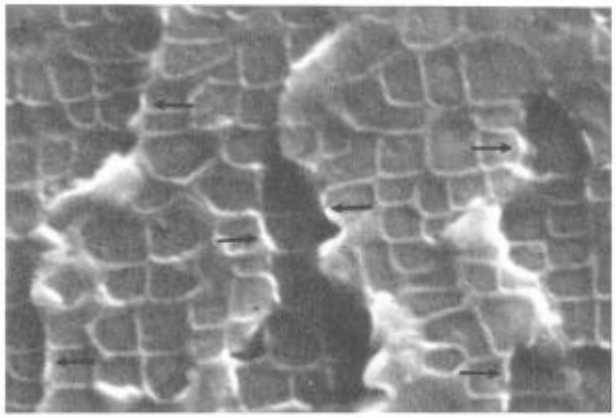

Fig. 7 Fatigue failure at ΔK of 2.2 MPa$\sqrt{m}$ in the mid-thickness. Arrows point to matrix failure.

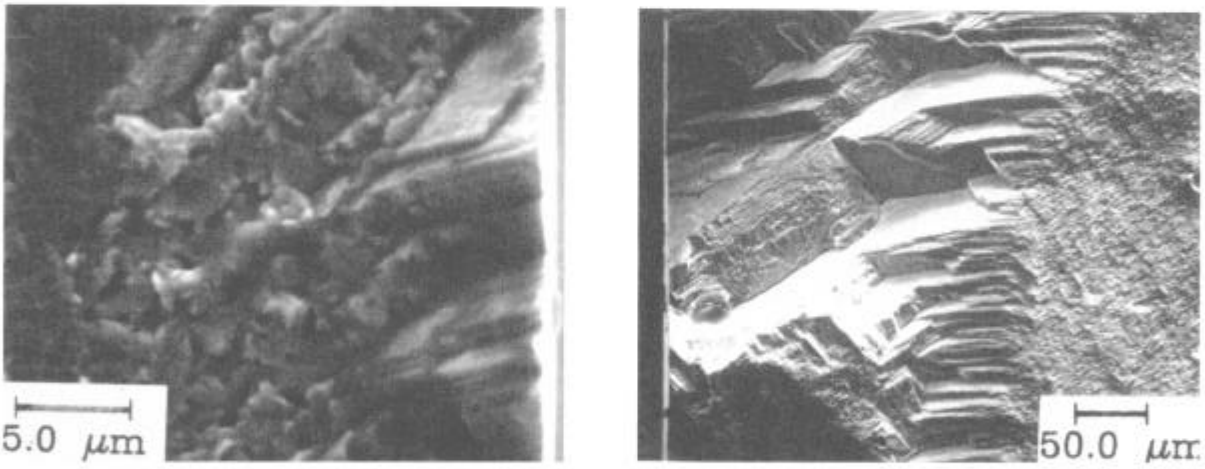

a) ΔK= 4 MPa$\sqrt{m}$ b) ΔK= 18.5 MPa$\sqrt{m}$

Fig. 8 {111} failure facets near outside surface.

The crystallographic planes on which fatigue failure occurred were not only dependent on the applied stress intensity but also on the through-thickness location. Near the outside surface, in the lower ΔK region, there was still an area approximately 5-10 μm thick of {111} failure (Fig. 8a). At somewhat higher stress intensities the regions of {111} failure extended deeper into the thickness, with the (001) regions being confined to small mid-thickness areas. The size of {111} facets was largest near the outside surfaces and rapidly decreased with increasing distance from the outside surfaces (Fig. 8b). While the failure occurred on all four {111} planes in the mid-thickness, failure occurred on only two {111} planes in the near surface. The summary of the fractographic findings is shown in Table I.

Table I Observed failure planes as a function of the applied ΔK.

ΔK	Outside Surface	1/4 Thickness	Mid-thickness
MPa√m	(Plane Stress)		(Plane Strain)
2	(111)	(001)	(001)
2.3			(001)
3.1			(001)
4.3		(001)	(001)
4.9		(001)/(111)	(001)
6.4			(001)
6.8		(001)/(111)	
7.4	(111)		
7.7		(111)/(001)	
8.9			(001)/(111)
11.3	(111)	(111)	(111)/(001)
13	(111)	(111)	(111)/(001)
16	(111)		(111)
18.5			(111)
23.1			(111)
25.3			(111)
27.5			(111)
29.7			(111)

The changeover from a predominantly (001) fatigue failure to {111} occurs at a ΔK of 7 to 10 MPa√m, as seen in Table I. This corresponds closely to the stress intensity at which the transition from accelerated to a more typical FCG behavior occurs (Fig. 3). Thus the unusual FCG behavior is associated with the (001) fatigue failure mechanism.

Resolved Shear Stress Intensity Parameter

The newly proposed K_{rss} parameter was used to explain some of the aspects of the observed microscopic failure mechanisms and the associated FCG behavior.

Definition: The resolved shear stress intensity parameter, K_{rss}, is defined, following Chen and Liu formulation (6), as the limiting value of the resolved shear stress, τ_{rss}, multiplied by $\sqrt{2\pi r}$, as r approaches zero:

$$K_{rss} = \lim_{r \to 0} \tau_{rss} \sqrt{2\pi r} \qquad (1)$$

where r is the distance to the crack tip and τ_{rss} is defined as the projection of the stress tensor $[\sigma]$ on a plane whose outward normal is $\vec{n}$ in the direction of slip $\vec{b}$.

$$\tau_{rss} = \vec{b} \cdot [\sigma] \vec{n} \qquad (2)$$

Fatigue cracking is postulated to occur along slip systems which have the highest K_{rss} value.

In this study, the three dimensional stress state $[\sigma]$ is approximated from the two dimensional boundary integral solution, assuming the asymptotic singularity of the stress field, under plane stress and plane strain conditions. Values of K_{rss} for PWA 1480 are determined by projecting the stresses near the crack on the {111} planes in a particular slip direction. The calculated maximum ΔK_{rss} values as a function of the normalized crack length for constant load range testing are shown in Fig. 9. The results indicate that the magnitude of the plane stress ΔK_{rss} is always approximately twice that of plane strain.

Application to FCG: To check the validity of the resolved shear stress intensity factor, K_{rss}, for correlating FCG data, ΔK_{rss} was calculated and plotted versus the da/dN data and is shown in Fig. 10, together with the da/dN versus the mode I ΔK plot. The shape of the two curves is virtually identical. A linear relationship exists (on the log-log basis) between ΔK_{rss} and da/dN which is similar in nature to the classical Paris region. This shows that the ΔK_{rss} parameter is as good as the mode I ΔK for FCG data correlation. But the advantage of ΔK_{rss} lies in the ability to predict the actual microscopic fatigue fracture mechanisms, as described next.

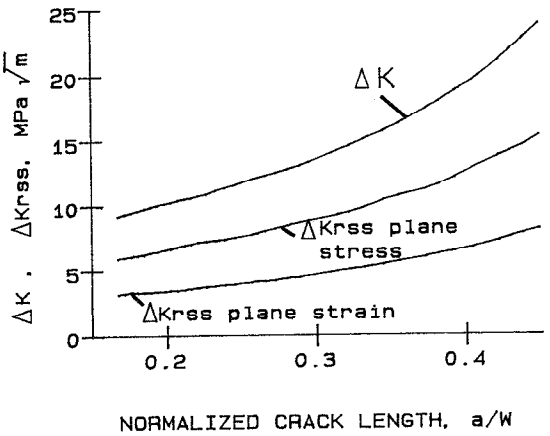

Fig. 9 Calculated values of ΔK_{rss} and ΔK as a function of crack length.

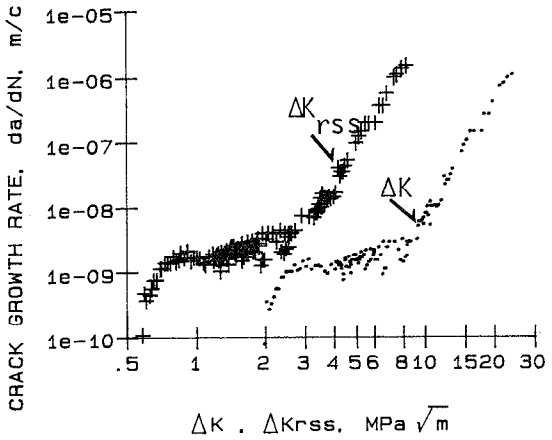

Fig. 10 Fatigue crack growth rate as a function of ΔK_{rss} and ΔK.

Prediction of the Microscopic Crack Behavior: An attempt was made to predict the microscopic crack path by the use of K_{rss} in the region where failure occurred on the {111} facets. It was assumed that the facets, through the entire thickness of the specimen, made either a 52° or -38° crack angle to the starter notch (taking into consideration the measured 7° macroscopic crack angle and in agreement with the observed slip surface traces). Table II shows the values of K_{rss} for different slip systems after a small amount of crack growth has occurred on either one of the crack angles, for both plane stress and plane strain conditions. Values in Table II can be used to predict whether the crack growth will continue in a self similar manner or change to a different slip system. For reference, the calculated Schmid factors are also given in the table.

Table II Normalized values of K_{rss} for different slip systems under plane stress and plane strain conditions.

			$K_{rss}b\sqrt{w}$ / P			
Slip Plane	Slip Direc.	Schmid Factor	Plane Stress -38°	Plane Stress 52°	Plane Strain -38°	Plane Strain 52°
(111)	[$\bar{1}$10]	.08	-1.77	-2.58	0.28	0.29
(111)	[$\bar{1}$01]	.34	2.24	0.10	2.56	0.55
(111)	[01$\bar{1}$]	.32	-3.97	-2.64	-2.28	-0.26
(1$\bar{1}$1)	[$\bar{1}$10]	.08	0.94	1.87	-0.69	-0.58
(1$\bar{1}$1)	[$\bar{1}$01]	.43	3.06	1.68	2.72	1.18
(1$\bar{1}$1)	[011]	.34	3.93	3.52	1.97	0.56
(11$\bar{1}$)	[1$\bar{1}$0]	.01	1.69	1.55	-0.63	-0.48
(11$\bar{1}$)	[101]	.42	-0.66	-2.32	-0.74	-2.38
(11$\bar{1}$)	[011]	.42	-2.30	-3.82	-0.13	-1.92
($\bar{1}$11)	[$\bar{1}$10]	.08	1.74	1.73	-0.86	-0.46
($\bar{1}$11)	[101]	.36	1.24	2.42	1.13	2.33
($\bar{1}$11)	[01$\bar{1}$]	.44	-3.05	4.25	-0.27	-1.91

First pairing systems of (1$\bar{1}$1) and ($\bar{1}$11)
Second pairing systems of (111) and (11$\bar{1}$)
Observed Failure Planes under Plane Stress Condition

For the plane strain case, the fractography of the mid-thickness region at intermediate ΔK_{rss} or (ΔK), showed that all four slip planes were active (Fig. 6b-d). A closer look at the fractography shows that the crack path zigzagged on two distinct pairs of planes (either ($\bar{1}$11) and (1$\bar{1}$1) or (111) and (11$\bar{1}$) as shown in Fig. 6c and d). The K_{rss} parameter can predict this type of crack growth behavior. For instance, after a small amount of crack growth at a 52° crack angle on the ($\bar{1}$11) plane in the [101] direction, the maximum K_{rss} changes to the (1$\bar{1}$1) plane in the [$\bar{1}$01] direction. Slip on this new system results in crack growth at a -38° crack angle. However after

a small extent of crack growth at the -38° crack angle, the maximum K_{rss} switches back to the original slip systems as seen in Table II. The same type of behavior occurs for the other pair of slip systems thus creating the observed fatigue crack behavior. For plane stress, after a small amount of crack growth at -38° on the $(\bar{1}11)$ $[01\bar{1}]$ system, the maximum normalized K_{rss} changes to (111) $[01\bar{1}]$ slip system, which results in the crack switching to the 52° inclination. The near surface failure was observed to occur on these two predicted planes. The surface slip offsets, as shown in Fig. 5b, suggest <011> slip direction in agreement with K_{rss} predictions. Presence of these two active slip systems suggests that cross slip might have been activated.

From the successful description of the FCG single crystal behavior, it can be concluded that the K_{rss} is a microscopic parameter that can quantify the crack driving force and at the same time be used to predict the microscopic crack propagation path under different stress states. K_{rss} can also be used to explain other aspects of the PWA 1480 single crystal behavior, as is described later on.

Relationship Between Slip Mechanisms and FCG Behavior

One of the main findings in this study was the identification of a relationship between the fatigue failure mode and the FCG behavior. Fatigue failure along {111} planes was associated with Paris region crack growth behavior, and along (001) planes was associated with the accelerated FCG behavior at low ΔK_{rss} (or ΔK). Accelerated FCG behavior refers to the comparison of the actually measured FCG rates versus the FCG rates obtained through the extrapolation of the Paris region to the low ΔK_{rss} region (Fig. 10). Examination of the effect of shear stresses on the dislocation motion in the matrix and in the γ' precipitates may explain this behavior.

It requires a certain critical value of the resolved shear stress, τ_o, to move a dislocation. The τ_o for dislocations to cut through the γ' precipitate is considerably higher than τ_o for dislocation motion through the matrix, as was shown by Copley and Kear (12). In the Paris region of Fig. 10 (intermediate ΔK_{rss} or ΔK), the shear stresses are high enough to allow for dislocations to slip through both the matrix and the precipitates (Fig. 5b). This process results in a {111} fatigue failure and the corresponding FCG behavior. However as ΔK_{rss} (or ΔK) is decreased, the accompanying resolved shear stresses also decrease. When the resolved shear stress falls below the critical value needed for a dislocation to cut through the precipitates, the slip becomes confined to the matrix. As mentioned earlier, the localization of the damage to the {111} matrix planes results in a preferential failure in that area, exposing the cuboidal facets of the precipitates and creating a (001) failure appearance. This scenario is supported by the previously mentioned fractographic evidence which indicated that the (001) failure appearance was associated with the observed failure in the matrix (Fig. 7). TEM will be performed to confirm this hypothesis.

The above hypothesis can be used to explain the accelerated FCG behavior encountered in the PWA 1480 at low stress intensities. The localization of the {111} slip to only the matrix will result in a higher local dislocation densities and increased dislocation interactions when compared to a situation where the dislocations can spread over a much longer active slip plane, as would be the case when both the matrix and the precipitates are sheared. For a given ΔK_{rss} (or ΔK), the localization of the slip exclusively to the matrix is a more damaging process than the one through which shearing of both the matrix and precipitates occurs. Therefore, at the lower ΔK_{rss} (or ΔK) the crack growth rates are higher than the extrapolated Paris region would predict.

The dependence of the failure mode on the state of stress, as shown previously in Table I, can be explained by reviewing the effect of stress state on the value of K_{rss}. As shown earlier, the plane stress K_{rss} is approximately twice that of plane strain (Fig. 9). The resolved shear stresses on the slip planes are directly proportional to the K_{rss} (eq. 1). Thus the resolved shear stresses on the dislocations are smaller in the mid-thickness (plane strain) than near the surface (plane stress) for a given crack length. The difference in the K_{rss} values, together with the previously postulated mechanism, explains the prevalence of (001) fatigue failure in the mid-thickness as compared to the more extensive {111} failure closer to the surface. The presence of considerably larger {111} surface facets which diminish rapidly with the distance from the outside surface (Fig. 8b), is due to a decrease in the K_{rss} caused by the change from plane stress near the surface to a mixed stress state away from the surface.

Conclusions

1. At ΔK greater than 8 MPa $\sqrt{m}$, the FCG rate exhibited the classical linear relation on a log-log basis between da/dN and ΔK (Paris region). In this region the microscopic crack propagation was along {111} slip planes. In the mid-thickness, all four planes were activated, however near the surface only two {111} slip planes were active.

2. At ΔK below 8 MPa$\sqrt{m}$, the FCG rate became almost independent of the applied ΔK. The change in the FCG behavior was related to a change in the fatigue failure mechanism. With the decrease in the applied ΔK, the (001) fatigue failure appearance became progressively more dominant.

3. The state of stress had a substantial influence on the fatigue failure mechanisms. At lower ΔK, while the (001) failure predominated in the mid-thickness regions, the near surface regions still exhibited {111} fatigue failure.

4. A mechanism was proposed, based on the barriers to dislocation motion, to explain the changes in the observed FCG behavior.

5. The FCG data was also evaluated in terms of a resolved shear stress intensity parameter, K_{rss}. This parameter, based on the shear stresses resolved into the slip planes, quantified the crack driving force as well as mode I ΔK, and at the same time predicted the crack path. The differences in the K_{rss} values were used to explain the observed dependence of the fatigue failure mode on the state of stress.

References

1. S. Pearson, Eng. Fract. Mech., vol 7, pp 235-247, 1975.
2. W.L. Morris, Met. Trans. A, vol 11, pp 1117-1123, July 1980.
3. J. Lankford, Fat. of Eng. Matl. and Struct., vol 5, no. 3, pp 233-248, 1982.
4. P. Newman and C.J. Beevers, R.O. Ritchie and J. Lankford eds., AIME, pp 97-116, 1986.
5. J. Telesman, D.M. Fisher and D. Holka, NASA TM 87208, 1985.
6. Q. Chen and H.W. Liu, NASA CR-182137, 1988.
7. R.V. Miner, J.Gayda and M.G. Hebsur, Low Cycle Fatigue, ASTM STP 942, pp. 371-384, 1988.
8. Standard Test Method for Measurement of Fatigue Crack Growth Rates, E 647, ASTM, 1987.
9. L.J. Ghosn, To appear in the ASME Journal of Tribology, vol 111, July 1988.
10. K.S. Chan and T.A. Cruse, Eng. Fract. Mech.,vol 23, no. 5, pp 863-874, 1986.
11. R.V. Miner, R.C. Voigt, J.Gayda and T.P. Gabb, Met. Trans., vol 17A, pp 491-496, 1986.
12. S.M. Copley and B.H. Kear, Trans. AIME, vol 239, pp 984-992, July 1967.